Fatigue Design of Steel Bridges Considering the Effect of Dynamic Vehicle Loading and Overloaded Trucks

Wei Wang[1]; Lu Deng, Ph.D., M.ASCE[2]; and Xudong Shao[3]

Abstract: The current practice for bridge-fatigue design may have underestimated the effect of dynamic vehicle loading and truck overloading on the fatigue life of steel bridges. In this study, a new approach for fatigue design of steel bridges was proposed that considers the effect of these two factors more rationally. A three-dimensional vehicle–bridge coupled model was developed to simulate the interaction between the bridge and vehicle. A simply supported steel I-girder bridge was used as an example for illustration of the proposed approach. The fatigue vehicle model was adopted from the AASHTO LRFD code, and overloading was considered by increasing the gross weight of the truck model. Numerical simulations were conducted to study the influence of three important parameters—road surface condition (RSC), vehicle speed, and truck gross weight—on the fatigue damage of the bridge considered. The results show that the RSC and truck gross weight both have a significant impact on the bridge-fatigue damage. By considering the cumulative fatigue damage caused by each truck passage under different RSCs and the deterioration process of the RSC during its whole lifecycle, a simple and reasonable expression was proposed for bridge-fatigue design. The proposed approach improves the current bridge-fatigue design method in that it rationally considers the vehicle dynamic effect, the influence of overloaded trucks, and the deterioration of RSC, which have a large influence on bridges' fatigue life. **DOI: 10.1061/(ASCE)BE.1943-5592.0000914.** *© 2016 American Society of Civil Engineers.*

Author keywords: Overloaded truck; Steel I-girder bridge; Fatigue damage; Road surface condition; Deterioration process.

Downloaded from ascelibrary.org by HUNAN UNIVERSITY on 11/07/16. Copyright ASCE. For personal use only; all rights reserved.

Introduction

Bridge components are subjected to repeated cyclic stresses with varying magnitude as a result of the dynamic vehicle loading during their lifecycles. The resulting fatigue damage can initiate cracks in steel bridge components and may cause fatigue failure. Worse still, vehicle overloading can greatly accelerate the fatigue-damage accumulation as a result of the large stress ranges induced. However, the current practice for bridge-fatigue design may underestimate the effect of dynamic vehicle loading and truck overloading on the fatigue life of steel bridges (Mohammadi and Polepeddi 2000; Polepeddi 1997).

Many studies have been conducted to investigate the effect of truck overloading on the fatigue behavior of steel bridges. Based on the weigh-in-motion (WIM) data, the statistical properties of overloaded trucks and the type of trucks that are more likely to cause bridge-fatigue damage were investigated by researchers (Mohammadi and Shah 1992; Wang et al. 2005; Zhao and Tabatabai 2012). Some researchers focused on how overloaded trucks affect the fatigue behavior of critical bridge components, such as welded cover plates and the assessment of service life reduction of steel bridges resulting from truck overload (Dicleli and Bruneau 1995; Polepeddi 1997). In addition, Mohammadi and Polepeddi (2000) incorporated the effect of overload on fatigue damage into bridge rating. However, those studies mainly focused on investigating how overload affects the fatigue behavior of in-service bridges, and little attention has been paid to considering the effect of overloaded trucks on the fatigue life of steel bridges from a design perspective.

The purpose of this paper is to propose a new approach for the fatigue design of steel bridges that can more rationally consider the vehicle dynamic effect and the influence of overloaded trucks. A simply supported steel I-girder bridge designed according to the AASHTO LRFD code (AASHTO 2012) was used to illustrate the proposed approach. First, a three-dimensional vehicle–bridge coupled model was developed to analyze the maximum stress ranges (MSRs, the algebraic difference between the maximum and minimum stresses) and corresponding equivalent number of stress cycles [ENSCs, as illustrated in Eq. (13)] induced by the passage of the fatigue truck currently adopted in the AASHTO LRFD code (AASHTO 2012) and by the overloaded trucks that have different gross weights, respectively. Then, a comparison between the fatigue damage induced by the passage of the design fatigue truck and that by the overloaded trucks was conducted. Finally, by considering the cumulative fatigue damage caused by each truck passage under different road surface conditions (RSCs) and the deterioration process of the RSC during its whole lifecycle, a simple and reasonable expression for fatigue design of steel bridges was proposed. The proposed approach improves the current bridge-fatigue design method by more rationally considering the vehicle dynamic effect, the influence of overloaded trucks, and the deterioration of RSCs, which have a large influence on bridges' fatigue life.

Analytical Bridge Model

In this study, a typical simply supported steel bridge designed according to the AASHTO LRFD code (AASHTO 2012) was adopted as an example for illustration of the proposed approach. This bridge consists of five identical I-girders with a spacing of

[1]Graduate Student, College of Civil Engineering, Hunan Univ., Changsha, Hunan 410082, China. E-mail: jswnww@hnu.edu.cn

[2]Professor, Key Laboratory for Wind and Bridge Engineering of Hunan Province, Hunan Univ., Changsha, Hunan 410082, China (corresponding author). E-mail: denglu@hnu.edu.cn

[3]Professor, Key Laboratory for Wind and Bridge Engineering of Hunan Province, Hunan Univ., Changsha, Hunan 410082, China. E-mail: shaoxd@hnu.edu.cn

Note. This manuscript was submitted on October 12, 2015; approved on January 27, 2016; published online on March 10, 2016. Discussion period open until August 10, 2016; separate discussions must be submitted for individual papers. This paper is part of the ***Journal of Bridge Engineering***, © ASCE, ISSN 1084-0702.

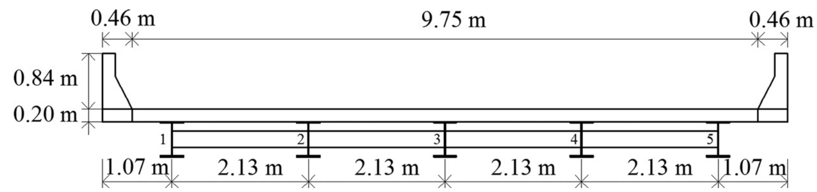

Fig. 1. Cross section of the bridge studied

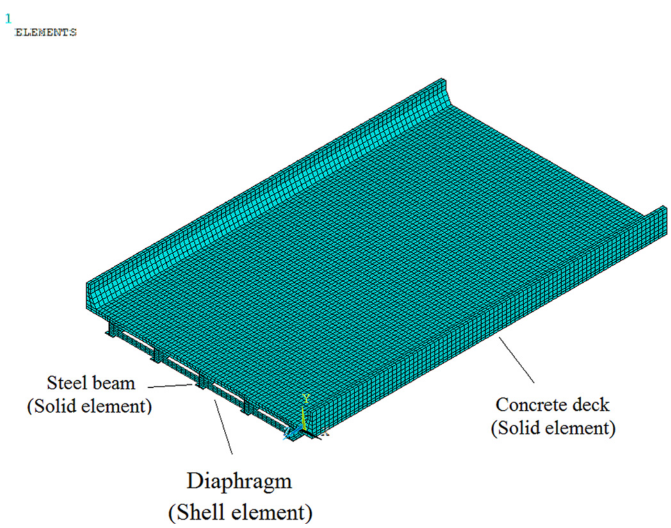

Fig. 2. Finite-element model of the bridge studied

2.13 m (7 ft). It has a span length of 16.76 m (55 ft), roadway width of 9.75 m (32 ft), and deck thickness of 0.20 m (8 in). The cross section of the bridge is shown in Fig. 1. In addition to the end diaphragms, two intermediate diaphragms were also used to achieve better distribution of the live load. The steel I-girders have a height of 1.61 m, cross-sectional area of 0.02 m^2, and moment of inertia of 0.0011 m^4. In the present study, the steel I-girder bridge was modeled with the *ANSYS 14.5* program, as shown in Fig. 2. The concrete bridge deck and guardrail were modeled by solid elements, whereas the steel girders and diaphragms were modeled by shell elements. The asphalt pavement and the dead weight of other elements (e.g., waterproof layer, drainage facilities) were not considered in this study, as these factors have a negligible effect on the fundamental frequency and vibration of the bridge structure (Wang et al. 2005; Zhang and Cai 2012). The fundamental frequency of the bridge obtained from the modal analysis using *ANSYS* is 8.62 Hz.

Analytical Vehicle Model

A fatigue truck is typically used to represent the equivalent fatigue damage accumulation resulting from truck traffic, which consists of trucks with a variety of gross vehicle weights and axle configurations at a specific site (Chotickai and Bowman 2006). The AASHTO fatigue guide specifications (AASHTO 1990) provide a single fatigue truck for the fatigue evaluation of steel bridges. The gross weight of the fatigue truck was stipulated to be 240 kN (54 kips) for the fatigue strength evaluation based on the actual truck traffic spectrum obtained from the WIM studies, through which data for more than 27,000 trucks and 30 sites around the United States (Snyder et al. 1985) were collected. The axle spacings (front and rear) of the fatigue truck are 4.27 and 9.14 m (14 and 30 ft), respectively, whereas the truck width is 1.83 m (6 ft). This truck configuration was developed based on the axle weight ratios and axle spacings of the four- and five-axle trucks, which were the main types of trucks that cause the fatigue damage of typical bridges (Schilling and Klippstein 1978). The current AASHTO LRFD code (AASHTO 2012) provides a similar truck for bridge-fatigue design, but the truck gross weight was increased to 320 kN (72 kips).

Based on the study by Mohammadi and Shah (1992), the majority of overloaded trucks were five-axle trucks. However, the average gross weight of overloaded trucks has been gradually increasing (Chotickai and Bowman 2006; Zhao and Tabatabai 2012). Therefore, in addition to the gross weight of 320 kN currently used for the fatigue truck in the AASHTO LRFD code (AASHTO 2012), five other values of gross weight that represent a typical weight range of overloaded trucks (Mohammadi and Shah 1992)—namely, 356 kN (80 kip), 400 kN (90 kip), 445 kN (100 kip), 489 kN (110 kip), and 534 kN (120 kip)—were adopted to investigate the effect of overload on the fatigue behavior of steel bridges. For convenience, the trucks with gross weights of 320, 356, 400, 445, 489, and 534 kN are represented by T_i ($i = 0$, 1, 2, 3, 4, 5) hereafter, respectively.

The HS20-44 truck specified in the AASHTO LRFD code (AASHTO 2012) was used as the fatigue truck in the present study. The analytical model for the fatigue truck is illustrated in Fig. 3. The properties of the truck, including the geometry, mass distribution, damping, and stiffness of the tires and suspension systems, are shown in Table 1. These truck parameters were derived based on the nationwide surveyed truck data (Wang and Huang 1993) and have been adopted as the parameters for the HS20-44 truck specified in the AASHTO LRFD code (AASHTO 2012) by many researchers (Wang and Liu 2000; Shi et al. 2008; Zhang and Cai 2013). It should be noted that, in this study, overload was considered by increasing the gross weight of the truck model only while the configuration and other parameters of the fatigue truck were kept unchanged. The purpose of doing this was to avoid making the problem too complicated, although in real life the parameters of trucks may vary with the truck type and their gross weights. The AASHTO LRFD code (AASHTO 2012) states that the fatigue load in fatigue design shall be one design truck, without considering the scenario involving multiple trucks present on the bridge, which has actually been considered when developing the fatigue truck.

Vehicle–Bridge Coupled System

Equation of Motion of Vehicle

The equation of motion for a vehicle can be expressed as follows:

$$[M_v]\{\ddot{d}_v\} + [C_v]\{\dot{d}_v\} + [K_v]\{d_v\} = \{F_G\} + \{F_v\} \tag{1}$$

where M_v, C_v, and K_v = mass, damping, and stiffness matrices of the vehicle, respectively; $\{d_v\}$ = the displacement vector of the

Downloaded from ascelibrary.org by HUNAN UNIVERSITY on 11/07/16. Copyright ASCE. For personal use only; all rights reserved.

Downloaded from ascelibrary.org by HUNAN UNIVERSITY on 11/07/16. Copyright ASCE. For personal use only; all rights reserved.

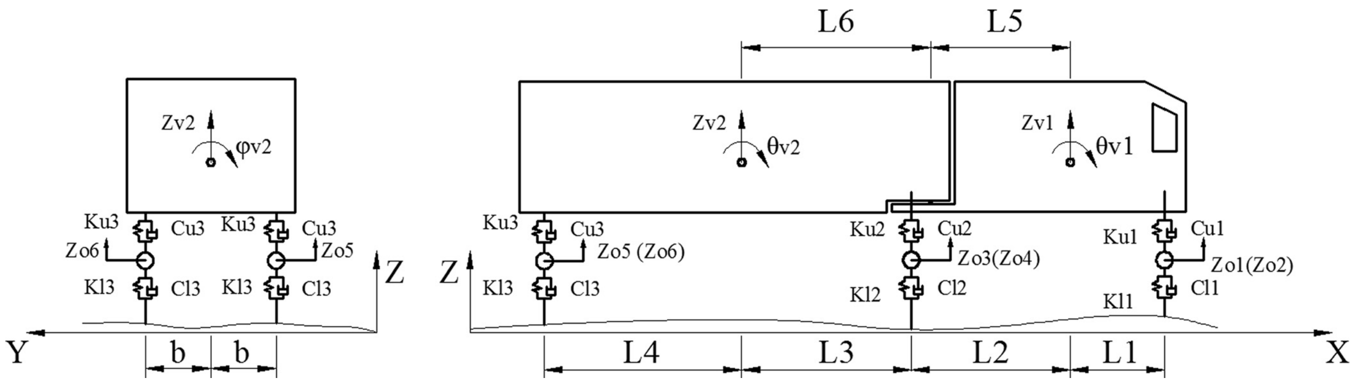

Fig. 3. Analytical model of the fatigue truck

Table 1. Main Parameters of Fatigue Truck Model Used in Study

Item	Parameter	Value
Mass	Truck body 1	2,612 (kg)
	Truck body 2	26,113 (kg)
	First axle suspension	490 (kg)
	Second axle suspension	808 (kg)
	Third axle suspension	653 (kg)
Geometry	L1	1.698 (m)
	L2	2.569 (m)
	L3	4.452 (m)
	L4	4.692 (m)
	L5	2.215 (m)
	L6	4.806 (m)
	B	1.1 (m)
Moment of inertia	Pitching, truck body1	2,022 (kg·m^2)
	Rolling, tuck body 1	8,544 (kg·m$^{2)}$
	Pitching, truck body2	33,153 (kg·m^2)
	Rolling, tuck body 2	181,216 (kg·m^2)
Spring stiffness	Upper, first axle	242,604 (N/m)
	Lower, first axle	875,082 (N/m)
	Upper, second axle	1,903,172 (N/m)
	Lower, second axle	3,503,307 (N/m)
	Upper, third axle	1,969,034 (N/m)
	Lower, third axle	3,507,429 (N/m)
Damper coefficient	Upper, first axle	2,190 (N·s/m)
	Lower, first axle	2,000 (N·s/m)
	Upper, second axle	7,882 (N·s/m)
	Lower, second axle	2,000 (N·s/m)
	Upper, third axle	7,182 (N·s/m)
	Lower, third axle	2,000 (N·s/m)

vehicle; $\{F_G\}$ = gravity force vector of the vehicle; and $\{F_v\}$ = the vector of wheel–road contact forces acting on the vehicle.

Equation of Motion of Bridge

The equation of motion for a bridge can be written as follows:

$$[M_b]\{\ddot{d}_b\} + [C_b]\{\dot{d}_b\} + [K_b]\{d_b\} = \{F_b\} \tag{2}$$

where M_b, C_b, and K_b = mass, damping, and stiffness matrices of the bridge, respectively; $\{d_b\}$ = displacement vector of the bridge; and $\{F_b\}$ = vector of wheel–road contact forces acting on the bridge.

Assembling the Vehicle–Bridge Coupled System

Based on the displacement relationship and the interaction force relationship at the contact points, the vehicle–bridge coupled system can be established by combining the equations of motion for both the bridge and vehicle, shown as follows:

$$\begin{bmatrix} M_b & \\ & M_v \end{bmatrix}\begin{Bmatrix} \ddot{d}_b \\ \ddot{d}_v \end{Bmatrix} + \begin{bmatrix} C_b + C_{b-b} & C_{b-v} \\ C_{v-b} & C_v \end{bmatrix}\begin{Bmatrix} \dot{d}_b \\ \dot{d}_v \end{Bmatrix} + \begin{bmatrix} K_b + K_{b-b} & K_{b-v} \\ K_{v-b} & K_v \end{bmatrix}\begin{Bmatrix} d_b \\ d_v \end{Bmatrix} = \begin{Bmatrix} F_{b-r} \\ F_{v-r} + F_G \end{Bmatrix} \tag{3}$$

where C_{b-b}, C_{b-v}, C_{v-b}, K_{b-b}, K_{b-v}, K_{v-b}, F_{b-r}, and F_{v-r} are due to the wheel–road contact forces and are time-dependent terms.

The modal superposition technique can be used to reduce the required computational effort. With this technique, the displacement vector of the bridge ($\{d_b\}$) in Eq. (2) can be expressed as

$$\{d_b\} = [\{\Phi_1\} \quad \{\Phi_2\} \ldots \{\Phi_m\}]\{\xi_1 \quad \xi_2 \cdots \xi_m\}^T = [\Phi_b]\{\xi_b\} \tag{4}$$

where m = total number of modes used for the bridge; and $\{\Phi_i\}$ and ξ_i = ith mode shape of the bridge and the ith generalized modal coordinate, respectively. Each mode shape is normalized such that $\{\Phi_i\}^{\mathrm{T}}[M_b]\{\Phi_i\} = 1$ and $\{\Phi_i\}^{\mathrm{T}}[\mathrm{K}_b]\{\Phi_i\} = \omega_i^2$.

Assuming $[C_b]$ in Eq. (2) is equal to $[2\omega_i\eta_i M_b]$, where ω_i is the frequency of the i th mode of the bridge and η_i is the percentage of the critical damping for the i th mode of the bridge, Eq. (2) can then be simplified into the following:

$$[I]\{\ddot{\xi}_b\} + [2\omega_i\eta_i I]\{\dot{\xi}_b\} + [\omega_i^2 I]\{\xi_b\} = [\Phi_b]^T\{F_b\} \tag{5}$$

where $[I]$ = unit matrix.

Eq. (3) can then be simplified into the following:

$$\begin{bmatrix} I & \\ & M_v \end{bmatrix}\begin{Bmatrix} \ddot{\xi}_b \\ \ddot{d}_v \end{Bmatrix} + \begin{bmatrix} 2\omega_i\eta_i I + \Phi_b^T C_{b-b}\Phi_b & \Phi_b^T C_{b-v} \\ C_{v-b}\Phi_b & C_v \end{bmatrix}\begin{Bmatrix} \dot{\xi}_b \\ \dot{d}_v \end{Bmatrix} + \begin{bmatrix} \omega_i^2 I + \Phi_b^T K_{b-b}\Phi_b & \Phi_b^T K_{b-v} \\ K_{v-b}\Phi_b & K_v \end{bmatrix}\begin{Bmatrix} \xi_b \\ d_v \end{Bmatrix} = \begin{Bmatrix} \Phi_b^T F_{b-r} \\ F_{v-r} + F_G \end{Bmatrix} \tag{6}$$

Because of the fact that the vehicle–bridge coupled system in Eq. (6) only contains the modal properties of the bridge and the physical parameters of the vehicles, the complexity of solving the vehicle–bridge coupling equations is greatly reduced. A *MATLAB* program was developed to assemble the vehicle–bridge coupled system in Eq. (6) and solve it using the fourth-order Runge–Kutta method in the time domain. The time step was set to 0.001 s to achieve numerical convergence. More details about the bridge–vehicle coupled system and the solving process can be found in Deng and Cai (2010b). The accuracy and reliability of the used bridge–vehicle model were verified in other works (Deng and Cai 2010a, 2011), in which a series of field tests were conducted on an existing slab-on-girder concrete bridge, and the bridge deflections and strains at the midspan of the girders were measured and compared with the bridge responses obtained from the numerical simulations. The field-measured results and the numerical results agree with each other very well. It should be noted that the bridge–vehicle coupled system used in this study is a linear–elastic system, and it was therefore assumed that both the steel and concrete materials work in their linear–elastic ranges, even under overloaded trucks.

After obtaining the bridge dynamic responses, the stress vector can be obtained by

$$[S] = [E][B][d_b] \tag{7}$$

where $[E]$ = stress–strain relationship matrix and is assumed to be constant over the element; and $[B]$ = strain–displacement relationship matrix assembled with x, y, and z derivatives of the element shape functions.

RSC

RSC has a very important effect on the dynamic interaction between the bridge and vehicle. A road surface profile is usually assumed to be a zero-mean stationary Gaussian random process and can be generated through an inverse Fourier transformation based on a power spectral density (PSD) function (Dodds and Robson 1973), such as:

$$r(X) = \sum_{k=1}^{N} \sqrt{2\varphi(n_k)\Delta n} \cos\,(2\pi n_k X + \theta_k) \tag{8}$$

where θ_k = random phase angle uniformly distributed from 0 to 2π; $\varphi()$ = PSD function (m^3/cycle/m) for the road surface elevation; and n_k = wave number (cycle/m). In the present study, the following PSD function was used (Huang and Wang 1992):

$$\varphi(n) = \varphi(n_0)\left(\frac{n}{n_0}\right)^{-2} \quad (n_1 < n < n_2) \tag{9}$$

where n = spatial frequency (cycle/m); n_0 = discontinuity frequency of $1/2\pi$ (cycle/m); $\varphi(n_0)$ = roughness coefficient (m^3/cycle) whose value is chosen depending on the road condition; and n_1 and n_2 = lower and upper cutoff frequencies, respectively.

The International Organization for Standardization (ISO 1995) has proposed a road roughness classification index from A (very good) to H (very poor) based on different values of $\varphi(n_0)$. In this study, the classification of road roughness based on ISO (1995) was used. Values of 5×10^{-6}, 20×10^{-6}, 80×10^{-6}, 256×10^{-6}, and $1{,}280 \times 10^{-6}$ m^3/cycle were adopted for $\varphi(n_0)$ corresponding to very good, good, average, poor, and very poor RSCs, respectively. The bridge surface is generally considered as part of the road surface, and therefore the road roughness classification index has also been commonly used to describe the bridge surface roughness (Huang and Wang 1992; Liu et al. 2002). The road roughness classification index adopted in this study was based on road surface spectra developed by Dodds and Robson (1973).

Numerical Studies

In this section, based on the developed three-dimensional bridge–vehicle coupled model, numerical simulations were performed and parametric studies were carried out. Parameters that affect the behavior of the bridge and vehicle system have been studied extensively (Chang and Lee 1994; Liu et al. 2002; Yang et al. 1995). In the present study, the effects of three important parameters, including the RSC, vehicle speed, and gross weight of the overloaded truck, were investigated. The maximum stress ranges and corresponding equivalent number of stress cycles induced by the trucks considered were then obtained and used in the fatigue analysis.

A total of seven vehicle speeds ranging from 30 to 120 km/h with an interval of 15 km/h were considered, and five different RSCs based on ISO (1995) were studied (very good, good, average, poor, and very poor). The loading case specified in the AASHTO LRFD code (AASHTO 2012), as shown in Fig. 4, was adopted in this study, and six trucks, denoted by T_i (I = 0, 1, 2, 3, 4, 5) as defined previously, were used for the vehicle loading.

To minimize the bias resulting from the randomly generated road surface profile, for each specific case with a given vehicle speed and RSC, the vehicle–bridge interaction analysis was set to run 20 times with 20 sets of randomly generated road surface profiles under the given RSC. Twenty simulations are generally believed to be sufficient by researchers (Liu et al. 2002; Deng and Cai 2010b). Then, the average values of the 20 MSRs and ENSCs equivalent were calculated and used to investigate the relationships between the parameters and the MSR and ENSC, respectively.

Bridge components may experience complex stress cycles as a result of truck passages, and fatigue damage will accumulate. Based on Miner's rule (Miner 1945), the accumulated fatigue damage (AFD) is calculated as

$$\mathrm{AFD}(t) = \sum_i \frac{n_i}{N_i} \tag{10}$$

where n_i = actual number of stress ranges; and N_i = number of stress cycles required for the component to fail at the corresponding level of stress range, which is denoted by S_i. It should be noted that Miner's rule assumes a linear damage accumulation and does not consider the effect of the sequence of stress application, which has been demonstrated to have little influence on the accuracy of the model (Albrecht and Friedland 1979; Schilling et al. 1978). Fatigue failure occurs when AFD(t) reaches 1, a value for the limit state condition. According to the fatigue analysis approach specified in

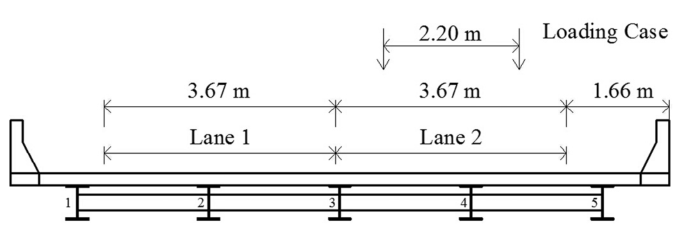

Fig. 4. Vehicle loading position

J. Bridge Eng., 2016, 21(9): 04016048

Downloaded from ascelibrary.org by HUNAN UNIVERSITY on 11/07/16. Copyright ASCE. For personal use only; all rights reserved.

the AASHTO LRFD code (AASHTO 2012), N_i and S_i hold the following relationship:

$$N_i = \frac{A}{S_i^m} \tag{11}$$

where A = fatigue–strength coefficient; and m = slope constant, which is usually taken as 3 for all AASHTO fatigue category details (Keating and Fisher 1986). It should be noted that there are inherent uncertainties in the parameters A and m. In fact, a confidence level of 95% was implicitly included in the design SN curves in the AASHTO LRFD code when adopting the values of the fatigue strength coefficient (A) and the slope constant (m) (Raju et al. 1990). Therefore, although these uncertainties were not explicitly expressed in the calculations in this study, the calculated fatigue damages should be viewed better as expected values rather than determinate values. Taking $m = 3$ and substituting Eq. (11) into Eq. (10), the following equation can be obtained:

$$\mathrm{AFD}(t) = \sum_i \frac{n_i S_i^3}{A} \tag{12}$$

During the passage of each truck, the complex stress cycles experienced by bridge components can be decomposed into the maximum stress cycles and one or more higher-order stress cycles (Schilling 1984). Fig. 5 shows the typical static and dynamic stress time-history curves at the midspan of Girder 4 of the bridge studied. The static stress curve (the dashed black line in Fig. 5) was obtained when the truck T_0 crosses the bridge at a crawling speed while the dynamic stress curve (the solid red line in Fig. 5) was obtained when Truck T_0 crossed the bridge under good RSC at a speed of 45 km/h. The algebraic difference between the maximum and minimum stresses is the MSR, as shown in Fig. 5.

Based on the results of the static MSRs at the midspan of all five girders of the bridge studied under the action of the 320-kN (72-kip) truck, it was found that the maximum static MSR (15.01 MPa) occurs at the midspan of Girder 4 for the bridge considered. Therefore, the stress at the midspan of Girder 4 was used for calculating the MSR and ENSC.

Fatigue details subjected to pure constant-amplitude loading would exhibit a fatigue limit (i.e., a stress range level below which fatigue failure would never occur during the design lifetime of the structure) (AASHTO 2012). However, Fisher et al. (1983) tested full-size specimens with various categories of fatigue details. They demonstrated that, if any of the stress ranges exceeds the constant-amplitude fatigue limit on the S–N curve, even by a small amount or by a small frequency, the fatigue life is not infinite anymore. In reality, vehicle loading has large uncertainties, and it is very likely the induced stress ranges will exceed the assumed fatigue limit during the design lifetime. Therefore, it is difficult to set a constant fatigue limit for estimating the fatigue life. To deal with this problem, in this study, every stress range induced by the fatigue truck was taken into account when considering the equivalent fatigue damage accumulation.

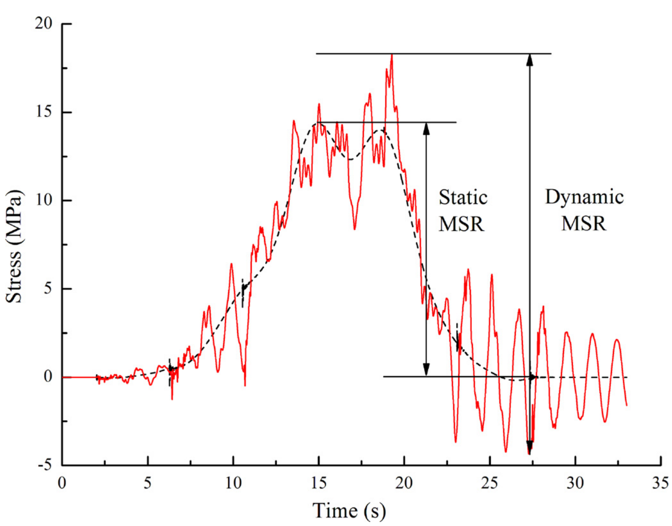

Fig. 5. Illustration of the maximum stress range

Based on the study by Schilling (1984), the cumulative fatigue damage resulting from the complex stress cycles caused by each truck passage can be represented by the fatigue damage resulting from the primary or maximum stress range with the ENSC determined from

$$\mathrm{ENSC} = \mathrm{num} + \left(\frac{S_{r1}}{S_{rm}}\right)^m + \left(\frac{S_{r2}}{S_{rm}}\right)^m + \cdots + \left(\frac{S_{ri}}{S_{rm}}\right)^m + \cdots + \left(\frac{S_{\mathrm{rcut}}}{S_{rm}}\right)^m \tag{13}$$

where num = number of maximum stress range induced by each truck passage; S_{rm} = maximum stress range; m = slope constant of the S–N curve; $S_{ri}(i = 1 \cdots \mathrm{cut})$ = higher-order stress ranges; and S_{rcut} = cutoff stress range used in the analysis. The slope constant (m) is approximately equal to 3 for all AASHTO fatigue category details (Keating and Fisher 1986). In the study, the stress ranges computed from the stress history were based on the rainflow counting algorithm (Downing and Socie 1982).

To illustrate how the RSC affects the MSR and ENSC, the stress time histories at the midspan of Girder 4 of the bridge studied under different RSCs are plotted in Fig. 6. It can be observed that the RSC has a significant effect on the MSR. It can also be observed that the RSC can also affect the high-order stress ranges and, therefore, the ENSC.

Based on Eq. (13), it is therefore necessary to determine a reasonable cutoff value when calculating the ENSC. In previous studies, for all welded details, the upper limit of a cutoff stress range is typically approximately 25–33% of the CAFL (Connor et al. 2004, 2005), whereas the applicable stress range cutoff levels could be within a range from 3.45 MPa (0.5 ksi) to 33% of the constant amplitude fatigue limit (CAFL) (Kwon et al. 2012; Kwon and Frangopol 2010). Therefore, the cutoff value for the stress range was 3.45 MPa (0.5 ksi) in this study.

Based on the numerical simulation results, the average MSRs and ENSCs of 20 simulations under the action of the trucks considered is plotted against vehicle speed in Figs. 7 and 8, respectively, where the results for trucks with different gross weights are plotted separately. As can be seen from Fig. 7, the average MSR is largely affected by the RSC and gross vehicle weight. The average MSR increases from 15.7 MPa under the action of Truck T_0 when the RSC is very good to 71.2 MPa under the action of Truck T_5 when the RSC is very poor. Fig. 8 shows that the ENSC is also greatly affected by the RSC. The ENSC can reach as large as 2.5 when the RSC is very poor, and can be less than 1.0 when the RSC is very good for all trucks considered.

Unlike the RSC and gross vehicle weight, an increase of vehicle speed does not necessarily result in a monotonic increase of the MSR and ENSC due to the fact that an increase of vehicle speed does not necessarily intensify the interaction between the bridge and vehicle, as reported by many other researchers (Brady

Downloaded from ascelibrary.org by HUNAN UNIVERSITY on 11/07/16. Copyright ASCE. For personal use only; all rights reserved.

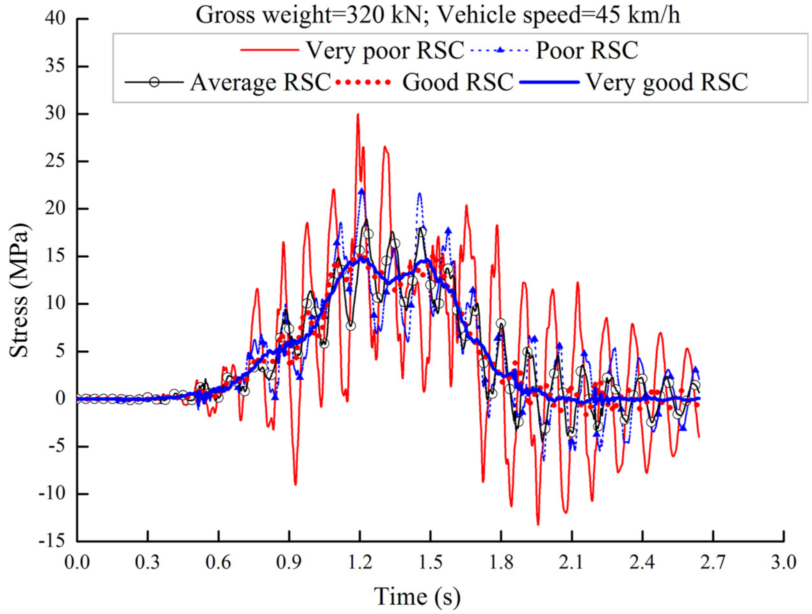

Fig. 6. Stress time histories at the midspan of Girder 4 of the bridge studied under different RSCs

et al. 2006; Liu et al. 2002). In addition, at a higher speed, the time required for the truck to pass the bridge is reduced, which leads to less time for bridge vibration in its higher-order modes. As a result, the total number of vibration cycles for higher-order modes is reduced, possibly resulting in a smaller ENSC.

Based on Eq. (12), the fatigue damage induced by each passage of the truck considered, T_i ($i = 0, 1, 2, 3, 4, 5$) under different RSCs (denoted by k hereafter, where $k = 1, 2, 3, 4$, and 5, representing very good, good, average, poor, and very poor RSCs, respectively) is defined as follows:

$$FD_{i,k} = \mathrm{ENSC}_{i,k} \cdot \mathrm{MSR}_{i,k}^3 \tag{14}$$

Based on Eq. (14), the fatigue damage induced by each passage of Truck T_0 under different RSCs is calculated using the results from Figs. 7 and 8, and the results are shown in Table 2. The ratios of the fatigue damage induced by the passage of each Truck T_i ($i = 1, 2, 3, 4, 5$) to that induced by Truck T_0 under different RSCs, denoted as $DR_{i,k}$, are summarized in Table 3.

Table 2 shows that the fatigue damage induced by the passage of Truck T_0 increases significantly as the RSC becomes worse, indicating that the RSC has a significant influence on the fatigue life of bridge components. Table 3 shows that the ratio of the fatigue damage induced by each passage of Truck T_i to that by Truck T_0 generally increases with the increase of the truck gross weight and decreases when the RSC becomes worse. In fact, the fatigue damage, as computed by Eq. (12), as well as the damage ratios are based on the calculated ENSC and MSR, both of which are influenced by all three parameters: RSC, vehicle speed, and gross weight of the overloaded truck. Therefore, their values are subjected to the cross influence of these three parameters and may not necessarily change monotonously with one specific parameter.

It should be noted that the results for each RSC in Tables 2 and 3 are obtained by taking the average of the fatigue damage for all seven vehicle speeds considered. The reason is that vehicles can run within a wide speed range, whereas an increase of vehicle speed does not always cause a monotonic increase or decrease of the MSR or ENSC. In addition, in real life, drivers tend to drive more slowly under poor RSCs; therefore, it may not be appropriate to calculate the average MSR and ENSC for poor RSC by taking the average of results for all seven vehicle speeds considered. However, because the effects of vehicle speed on the MSR and ENSC do not follow a monotonic increase or decrease trend, taking their average values should be fair when analyzing the results.

Based on the study by Zhang and Cai (2012), during a 15-year pavement maintenance cycle, the RSC usually stays in the class of *very good* in the first 8 years, *good* in the ninth and tenth years, *average* in the eleventh and twelfth years, *poor* in the thirteenth year, and *very poor* in the fourteenth and fifteenth years. In other words, during a 15-year maintenance cycle, the proportions of time that the RSC stays in each class (denoted by TR_k, $k = 1, 2, 3, 4, 5$) are 0.53, 0.13, 0.13, 0.067, and 0.13, respectively. During the assumed 75-year service life of bridges, the pavement on the bridge may undergo multiple maintenance cycles. Because these are repeated cycles, the proportion of time that the bridge surface stays in each level of RSC during the 75-year service life can be approximated by the proportion of time the bridge surface stays in each level of RSC during a 15-year pavement maintenance cycle. Considering the cumulative fatigue damage caused by each truck passage under different RSCs and the whole maintenance cycle of the RSC, the average fatigue damage induced by each passage of Truck T_i ($i = 1, 2, 3, 4, 5$) can be calculated as

$$FD_{(\mathrm{MC})i} = \sum_{k=1}^{5} FD_{i,k} \cdot TR_k \tag{15}$$

It should be emphasized that the term *average fatigue damage* specifically means the average fatigue damage caused by the passage of a truck with respect to different RSCs considering the time proportion of each class of RSC during a pavement maintenance cycle. Based on Eq. (15) and Table 2, the average fatigue damage caused by Truck T_0 [i.e., $FD_{(\mathrm{MC})0}$] is calculated to be 39,698 MPa^3 (120.8 ksi^3). The ratio of the average fatigue damage induced by each passage of Truck T_i ($i = 1, 2, 3, 4, 5$) to that by Truck T_0 during a pavement maintenance cycle, denoted by $DR_{(\mathrm{MC})i}$, is calculated by using Eq.(16), and the results are shown in Table 4

Downloaded from ascelibrary.org by HUNAN UNIVERSITY on 11/07/16. Copyright ASCE. For personal use only; all rights reserved.

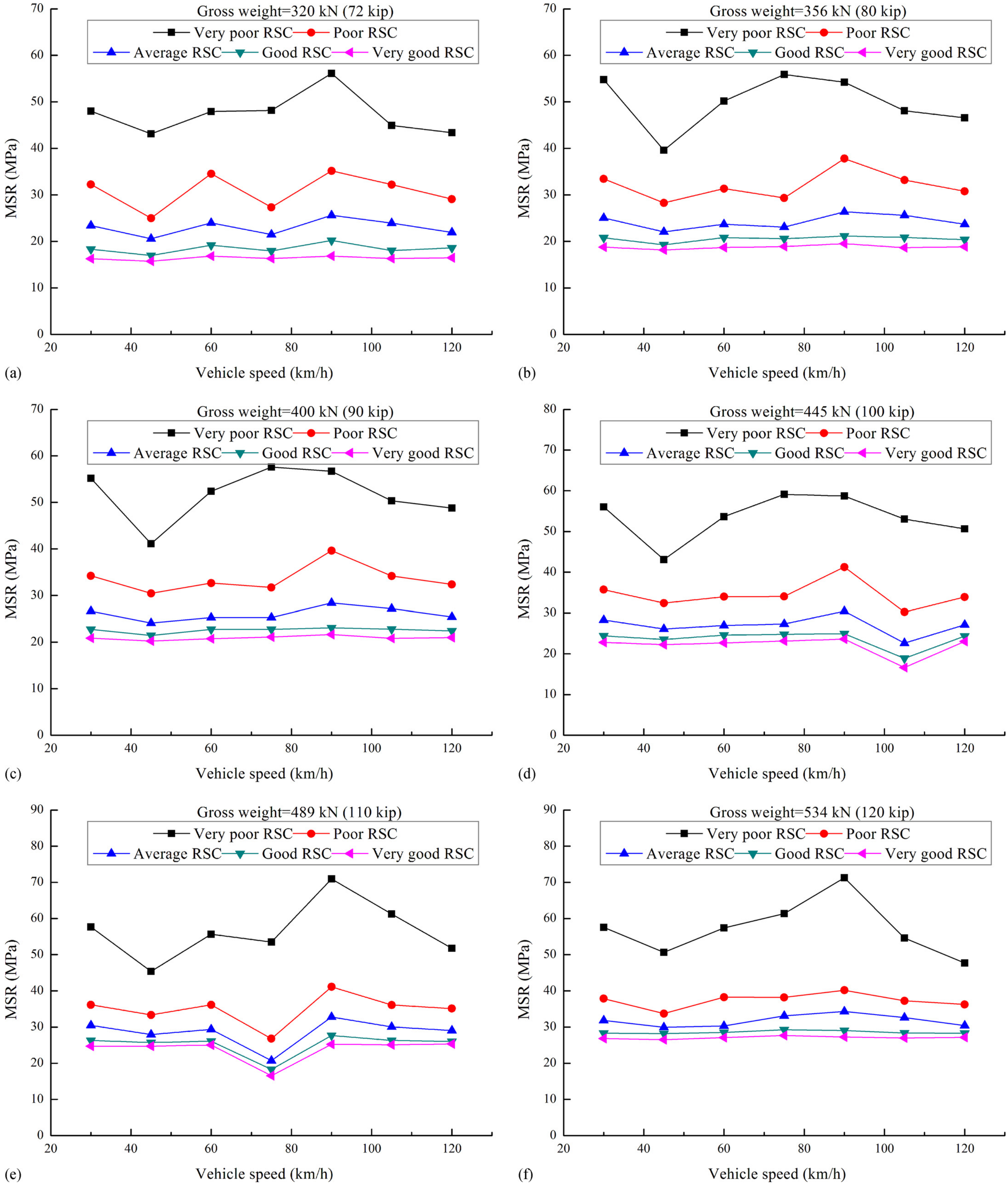

Fig. 7. Variation of MSR with change in vehicle speed and RSC for the trucks with different gross weights considered

Downloaded from ascelibrary.org by HUNAN UNIVERSITY on 11/07/16. Copyright ASCE. For personal use only; all rights reserved.

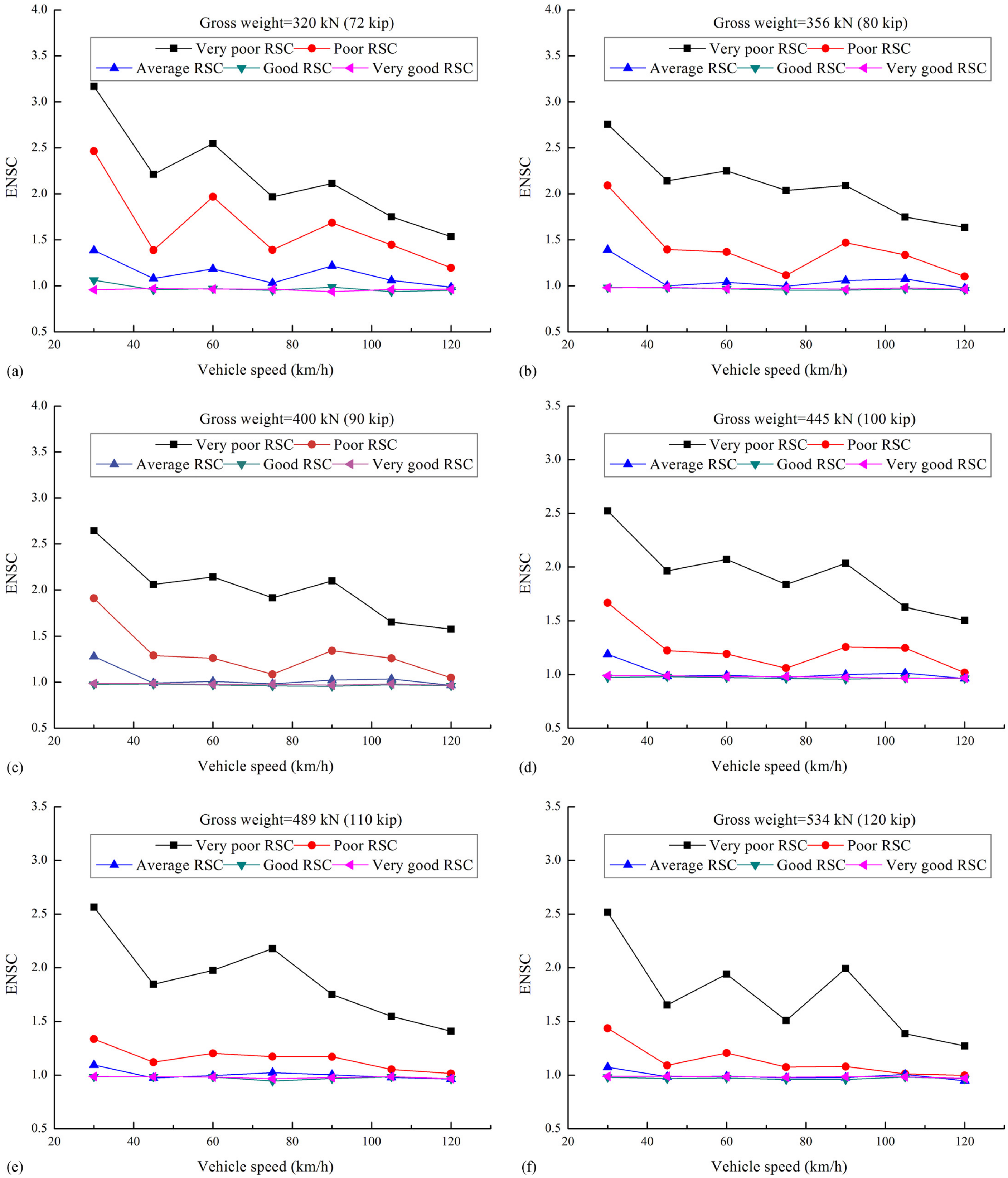

Fig. 8. Variation of ENSC with change in vehicle speed and RSC for the trucks with different gross weights considered

Downloaded from ascelibrary.org by HUNAN UNIVERSITY on 11/07/16. Copyright ASCE. For personal use only; all rights reserved.

Table 2. Fatigue Damage Induced by Each Passage of Truck T_0 under Different RSCs

RSC	FD_0 (MPa^3)
Very good	4,248.5
Good	6,200.2
Average	14,182.7
Poor	52,134.4
Very poor	240,796.3

Table 3. Ratio of Fatigue Damage Induced by Each Truck T_i (i = 1, 2, 3, 4, 5) to That by Truck T_0 under Different RSCs

	RSC				
Truck	Very good	Good	Average	Poor	Very poor
T_0	1.00	1.00	1.00	1.00	1.00
T_1	1.53	1.38	1.12	1.01	1.16
T_2	2.11	1.83	1.35	1.10	1.24
T_3	2.54	2.13	1.50	1.16	1.32
T_4	3.26	2.64	1.75	1.11	1.51
T_5	4.60	3.74	2.40	1.35	1.42

Table 4. Ratio of Fatigue Damage Induced by Each Passage of the Truck T_i (i = 0, 1, 2, 3, 4, 5) to That by Truck T_0 during a Pavement Maintenance Cycle

Truck	$DR_{(\mathrm{MC})i}$	$DRO_{(\mathrm{MC})i}$
T_0	1	11.74
T_1	1.35	15.85
T_2	1.77	20.78
T_3	2.07	24.30
T_4	2.57	30.17
T_5	3.51	41.21

$$DR_{(\mathrm{MC})i} = \sum_{k=1}^{5} DR_{i,k} \cdot TR_k \tag{16}$$

where $DR_{i,k}$ = ratio of the fatigue damage induced by Trucks T_i (i = 1, 2, 3, 4, 5) to that by Truck T_0 under different RSCs, as summarized in Table 3. To illustrate the effect of dynamic loading due to overloaded trucks on the fatigue life of steel bridges, the ratio of the average fatigue damage induced by each passage of Truck T_i (i = 1, 2, 3, 4, 5) considering dynamic load effect during a pavement maintenance cycle to that by Truck T_0 without considering dynamic effect, denoted by $DRO_{(\mathrm{MC})i}$, is also obtained and shown in Table 4.

Table 4 shows that when the dynamic loading effect is considered, the ratio of fatigue damage induced by the overloaded trucks to that induced by Fatigue Truck T_0 [i.e., $DR_{(\mathrm{MC})i}$] increases from 1.00 to 3.51, whereas the truck weight ratio increases from 1.00 (= 320/320 kN) to 1.67 (= 534/320 kN). This increase of fatigue damage ratio with increasing truck weight ratio demonstrates the effect of truck overloading on the fatigue damage caused, whereas the effect of dynamic vehicle loading on fatigue damage can be illustrated by the fatigue damage ratio between two cases with and without considering the dynamic vehicle loading effect, which reaches 11.74 as shown in Table 4. Therefore, the results in Table 4 indicate the importance of considering the dynamic vehicle loading effect of overloaded trucks in the fatigue design or evaluation of steel bridges.

Proposed Approach for Fatigue Design

Studies have shown that the gross weight of overloaded trucks has increased compared to when the fatigue truck was developed (Mohammadi and Shah 1992; Zhao and Tabatabai 2012). To reflect this increase of vehicle gross weight, and to account for the effect of the RSC, a new approach for bridge-fatigue design is proposed.

In the following analysis, N_{T0} is used to denote the number of the daily passage of the fatigue truck (T_0) used in the fatigue design, and NR_i is used to denote the ratio of the increasing number of the overloaded trucks [i.e., T_i (i = 1, 2, 3, 4, 5)] to the number of Fatigue Truck T_0. The traffic increase by year was not considered in the study. Based on Eq. (12), during a 75-year design period, the accumulative fatigue damage induced by all of the trucks considered [i.e., T_i (i = 0, 1, 2, 3, 4, 5)] can be calculated as

$$\mathrm{AFD}(t) = \frac{n_0 S_0^3}{A} + \frac{n_1 S_1^3}{A} + \cdots + \frac{n_5 S_5^3}{A} \tag{17}$$

where $n_i S_i^3 = 75 \cdot 365 \cdot N_{Ti} \cdot FD_{(\mathrm{MC})i}$; and N_{Ti} = number of daily passages of Truck T_i, and can be simply calculated as $N_{Ti} = N_{T0} \cdot NR_i$, where i = 1, 2, 3, 4, 5.

Substituting $n_i S_i^3$ into Eq. (17), the following can be obtained:

$$\begin{aligned}\mathrm{AFD}(t) &= \frac{75 \cdot 365 \cdot N_{T0} \cdot FD_{(\mathrm{MC})0}}{A} + \frac{75 \cdot 365 \cdot N_{T1} \cdot FD_{(\mathrm{MC})1}}{A} \\ &\quad + \cdots + \frac{75 \cdot 365 \cdot N_{T5} \cdot FD_{(\mathrm{MC})5}}{A} = 27,375 \\ &\quad \times \left(\frac{N_{T0} \cdot FD_{(\mathrm{MC})0}}{A} + \frac{NR_1 \cdot N_{T0} \cdot DR_{(\mathrm{MC})1} \cdot FD_{(MC)0}}{A}\right. \\ &\quad \left. + \cdots + \frac{NR_5 \cdot N_{T0} \cdot DR_{(\mathrm{MC})5} \cdot FD_{(\mathrm{MC})0}}{A}\right) = 27,375 \\ &\quad \times (1 + NR_1 \cdot DR_{(\mathrm{MC})1} + \cdots + NR_5 \cdot DR_{(\mathrm{MC})5}) \\ &\quad \times \frac{N_{T0} \cdot FD_{(\mathrm{MC})0}}{A}\end{aligned} \tag{18}$$

During a 75-year lifecycle, the accumulative fatigue damage should be no greater than 1. Therefore, the following equation should hold:

$$\begin{aligned}&27,375(1 + NR_1 \cdot DR_{(\mathrm{MC})1} + \cdots + NR_5 \cdot DR_{(\mathrm{MC})5}) \\ &\quad \times \frac{N_{T0} \cdot FD_{(\mathrm{MC})0}}{A} \leq 1\end{aligned} \tag{19}$$

which leads to the following:

$$\begin{aligned}&(1 + NR_1 \cdot DR_{(\mathrm{MC})1} + \cdots + NR_5 \cdot DR_{(\mathrm{MC})5}) N_{T0} \\ &\quad \leq \frac{A}{27,375 FD_{(\mathrm{MC})0}}\end{aligned} \tag{20}$$

It can be easily seen that Eq. (20) can account for different truck compositions in traffic, in terms of gross weight, by means of using different truck ratios [NR_i (i = 1, 2, 3, 4, 5)].

To determine the daily allowable number of Fatigue Truck T_0, the ratios of the increasing number of overloaded Trucks T_i to that of Fatigue Truck T_0 [i.e., NR_i (i = 1, 2, 3, 4, 5) in Eq. (20)] need to be determined first. Table 5 shows the weight distribution of the surveyed trucks based on which fatigue design truck was developed

Downloaded from ascelibrary.org by HUNAN UNIVERSITY on 11/07/16. Copyright ASCE. For personal use only; all rights reserved.

(Schilling and Klippstein 1977). Assuming that the increase in traffic volume is not considered, the increase in the number of overloaded trucks will lead to a decrease in the percentage of trucks with relatively light weight and an increase in the percentage of relative heavy trucks. Because a small decrease in the number of relatively lightweight trucks will only have a negligible impact on fatigue life of steel bridges, only the effect of the increasing percentage of overloaded trucks was considered, whereas the effect of the reduced number of relatively lightweight trucks on the fatigue life was not considered. This leads to a slightly more conservative result on the predicted allowable number of fatigue trucks. Fig. 9 shows an example of change in truck composition, in terms of gross vehicle weight, used in the present study.

To illustrate the difference between the proposed approach and the current fatigue design method adopted by the AASHTO LRFD code (AASHTO 2012), two examples were used in this section to compare the maximum daily allowable number of truck passages predicted by the proposed approach and the current AASHTO LRFD code (AASHTO 2012) to achieve a 75-year design life.

The change of truck composition shown in Table 5 was assumed for the first example, whereas in the second example, no overloads were considered [i.e., the parameters, $DR_{(\mathrm{MC})i}$ (i = 1, 2, 3, 4, 5), in Eq. (20) all equal 0]. For the determination of the fatigue–strength coefficient (A), because the welded cover plates of the steel girders were the details focused on in this study, a fatigue–strength coefficient of 120×10^8 ksi^3 (3.93×10^{12} MPa^3)was taken, which corresponds to Category B (Item 3.1, i.e., welds between the bottom flange and the plate) for welded joints, as specified in the AASHTO LRFD code (AASHTO 2012). A 15-year pavement maintenance cycle used by Zhang and Cai (2012) was assumed in calculating the average fatigue damage caused by each truck passage. Based on Eq. (20), the maximum allowable N_{T0} for the first example was calculated to be 3,135. Therefore, based on the assumed truck composition, the total number of daily passages of trucks, including overloaded trucks, was calculated to be 3,440. Similarly, the total number of daily passages of trucks for the second example was calculated to be 3,629. A comparison between these two examples shows that a larger proportion of overloaded trucks will result in a smaller maximum daily allowable number of truck passages.

In the current AASHTO LRFD code (AASHTO 2012), for load-induced fatigue consideration, each detail shall satisfy

$$\gamma(\Delta f) \leq \left(\frac{A}{365 \times 75 \times n \times (\mathrm{ADTT})_{\mathrm{SL}}}\right)^{\frac{1}{3}} \tag{21}$$

where γ = load factor for the fatigue load combination, taken as 0.75; Δf = live load stress range resulting from the passage of the fatigue truck; A = fatigue–strength coefficient, which is taken as 120×10^8 ksi^3 (3.93×10^{12} MPa^3); n = number of stress range cycles induced by each truck passage, taken as 1 for the bridge considered; and $(\mathrm{ADTT})_{\mathrm{SL}}$ = number of single-lane daily passages of trucks. Δf is calculated to be 17.26 MPa (2.50 ksi) for the bridge girder considered, including a dynamic impact factor of 0.15 as specified in the AASHTO LRFD code (AASHTO 2012). Based on Eq. (21), the maximum allowable value of $(\mathrm{ADTT})_{\mathrm{SL}}$ is calculated to be 66,368.

Through comparison, it is obvious that the maximum daily allowable number of truck passages obtained by the current LRFD code is almost 20 times as large as that predicted by the proposed approach, indicating that dynamic vehicle loading and overloaded

Table 5. Illustration of How to Calculate Increasing Percentage of Overloaded Trucks

Truck weight [kN (kip)]	Percentage: Schilling and Klippstein (1977)	Percentage: Example	Percentage: Increase
<112 (<25)	1.52	0.80	–0.72
112–222 (25–49)	33.94	27.94	–6.00
223–244 (50–74)	40.40	37.40	–3.00
334–378 (75–84)	22.75	26.75	6.00
379–422 (85–94)	1.34	3.34	2.00
423–467 (95–104)	0.039	1.039	1.00
468–511 (105–114)	0.0046	0.5046	0.50
>512 (>115)	0.0009	0.2209	0.22

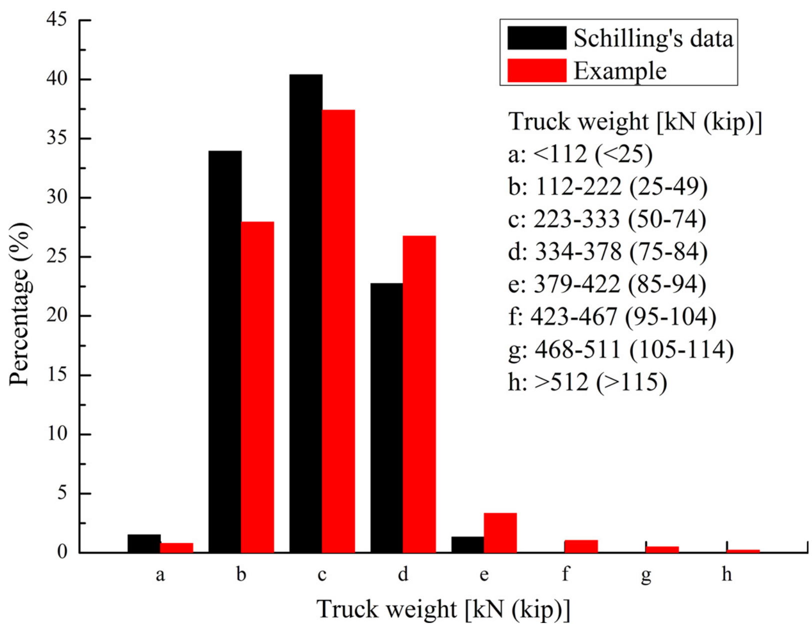

Fig. 9. Illustration of the change in truck composition in terms of gross vehicle weight

Downloaded from ascelibrary.org by HUNAN UNIVERSITY on 11/07/16. Copyright ASCE. For personal use only; all rights reserved.

trucks together have a significant effect on the fatigue life of steel bridges and should be considered wherever appropriate in the fatigue design or evaluation of steel bridges.

It should be noted that, although the results in the previous section were based on two examples, the proposed method can be applied to different bridge components under different situations. The procedures to implement the new approach can be summarized as follows:

1. Obtain or assume the truck composition of the traffic condition to be considered and compare it with the weight distribution of the trucks in the original survey (in Table 5) to quantify the weight increase of overloaded trucks in terms of percentage increase of truck numbers within each weight level.
2. Obtain the maximum stress range and corresponding equivalent number of stress ranges experienced by the bridge component to be considered under different RSCs while considering the effect of dynamic vehicle loading and the overloaded trucks through a bridge–vehicle interaction analysis.
3. Obtain the relationship between the fatigue damage induced by each passage of the fatigue design truck and that by the overloaded trucks with different gross weights under different RSCs.
4. Adopt or assume a RSC deterioration model and calculate the average fatigue damage induced by each truck passage during the whole lifecycle of the RSC; then, obtain the relationship of the average fatigue damage caused by each passage of the fatigue design truck and that by the overloaded trucks with different gross weights.
5. Based on Miner's fatigue accumulation rule and all the knowns obtained in previous steps, Eq. (18) can then be used to predict the allowable daily passage of fatigue truck that can achieve the target fatigue life by the code.

Summary and Conclusions

A new approach for the fatigue design of steel bridges was proposed in this study with the aim of accurately considering the effect of dynamic vehicle loading and truck overloading on the fatigue life of steel bridges. A typical simply supported steel bridge was adopted as an example in this study. The relationship between the fatigue damage induced by each passage of overloaded trucks and that by the fatigue design truck was investigated under two cases with and without considering the dynamic vehicle loading effect. Based on the study, the following conclusions can be drawn:

1. During a pavement maintenance cycle, the ratio of average fatigue damage induced by a 534-kN overloaded truck to that induced by a 320-kN fatigue truck reaches 3.51 even though their weight ratio is only 1.67.
2. The average fatigue damage induced by a truck when considering the dynamic vehicle loading effect can be 11.74 times as large as that without considering the dynamic vehicle loading effect.
3. The overloaded trucks together with poor RSCs have a great impact on the fatigue life of steel bridges. In the current AASHTO LRFD code (AASHTO 2012), the effect of dynamic vehicle loading on the fatigue life of steel bridges may be underestimated, leading to an overestimation of fatigue life of steel bridges.

The results from this study highlight the importance of considering the effect of dynamic vehicle loading and the overloaded trucks on the fatigue design of steel bridges. The proposed method can be used as a supplementation to the AASHTO LRFD code (AASHTO 2012) where the deterioration of RSC and truck overloading may raise attention. In this paper, the pavement maintenance cycle and deterioration process were assumed based on available literature. Future research could focus on studying the effect of the pavement maintenance cycle on the fatigue behavior of steel bridges and propose an optimal pavement maintenance plan based on the consideration of both maintenance cost and bridge-fatigue life.

Acknowledgments

The authors acknowledge the financial support provided by the National Natural Science Foundation of China (Grant Nos. 51208189 and 51478176) and the Excellent Youth Foundation of Hunan Scientific Committee (Grant No. 14JJ1014).

References

AASHTO. (1990). *Guide specifications for fatigue evaluation of existing steel bridges*, Washington, DC.

AASHTO. (2012). *AASHTO LRFD bridge design specifications*, 6th Ed., Washington, DC.

Albrecht, P., and Friedland, I. M. (1979). "Fatigue-limit effect on variable-amplitude fatigue of stiffeners." *J. Struct. Div.*, 105(12), 2657–2675.

ANSYS 14.5 [Computer software]. Ansys, Canonsburg, PA.

Brady, S. P., O'Brien, E. J., and Žnidarič, A. (2006). "Effect of vehicle velocity on the dynamic amplification of a vehicle crossing a simply supported bridge." *J. Bridge Eng.*, 10.1061/(ASCE)1084-0702(2006)11:2(241), 241–249.

Chang, D., and Lee, H. (1994). "Impact factors for simple-span highway girder bridges." *J. Struct. Eng.*, 10.1061/(ASCE)0733-9445(1994)120:3(704), 704–715.

Chotickai, P., and Bowman, M. (2006). "Truck models for improved fatigue life predictions of steel bridges." *J. Bridge Eng.*, 10.1061/(ASCE)1084-0702(2006)11:1(71), 71–80.

Connor, R., Hodgson, I., Mahmoud, H., and Bowman, C. (2005). *Field testing and fatigue evaluation of the I-79 Neville Island Bridge over the Ohio River*, Lehigh Univ. Center for Advanced Technology for Large Structural Systems, Bethlehem, PA.

Connor, R. J., Fisher, J. W., Hodgson, I. C., and Bowman, C. A. (2004). *Results of field monitoring prototype floorbeam connection retrofit details on the Birmingham Bridge*, Lehigh Univ. Center for Advanced Technology for Large Structural Systems, Bethlehem, PA.

Deng, L., and Cai, C. (2010a). "Bridge model updating using response surface method and genetic algorithm." *J. Bridge Eng.*, 10.1061/(ASCE)BE.1943-5592.0000092, 553–564.

Deng, L., and Cai, C. S. (2010b). "Development of dynamic impact factor for performance evaluation of existing multi-girder concrete bridges." *Eng. Struct.*, 32(1), 21–31.

Deng, L., and Cai, C. S. (2011). "Identification of dynamic vehicular axle loads: Demonstration by a field study." *J. Vib. Control*, 17(2), 183–195.

Dicleli, M., and Bruneau, M. (1995). "Fatigue-based methodology for managing impact of heavy-permit trucks on steel highway bridges." *J. Struct. Eng.*, 10.1061/(ASCE)0733-9445(1995)121:11(1651), 1651–1659.

Dodds, C., and Robson, J. (1973). "The description of road surface roughness." *J. Sound Vib.*, 31(2), 175–183.

Downing, S. D., and Socie, D. (1982). "Simple rainflow counting algorithms." *Int. J. Fatigue*, 4(1), 31–40.

Fisher, J. W., Mertz, D. R., and Zhong, A. (1983). "Steel bridge members under variable amplitude long life fatigue loading." *National Cooperative Highway Research Program Rep. 267*, Transportation Research Board, Washington, DC.

Huang, D., and Wang, T.-L. (1992). "Impact analysis of cable-stayed bridges." *Comput. Struct.*, 43(5), 897–908.

ISO (International Organization for Standardization). (1995). "Mechanical vibration—Road surface profiles—Reporting of measured data." *ISO 8068: (E)*, Geneva.

Downloaded from ascelibrary.org by HUNAN UNIVERSITY on 11/07/16. Copyright ASCE. For personal use only; all rights reserved.

Keating, P. B., and Fisher, J. W. (1986). "Evaluation of fatigue tests and design criteria on welded details." *National Cooperative Highway Research Program Rep. No. 286*, Transportation Research Board, Washington, DC.

Kwon, K., and Frangopol, D. M. (2010). "Bridge fatigue reliability assessment using probability density functions of equivalent stress range based on field monitoring data." *Int. J. Fatigue*, 32(8), 1221–1232.

Kwon, K., Frangopol, D., and Soliman, M. (2012). "Probabilistic fatigue life estimation of steel bridges by using a bilinear S-N approach." *J. Bridge Eng.*, 10.1061/(ASCE)BE.1943-5592.0000225, 58–70.

Liu, C., Huang, D., and Wang, T.-L. (2002). "Analytical dynamic impact study based on correlated road roughness." *Comput. Struct.*, 80(20), 1639–1650.

MATLAB [Computer software]. MathWorks, Natick, MA.

Miner, M. A. (1945). "Cumulative damage in fatigue." *J. Appl. Mech.*, 12(3), 159–164.

Mohammadi, J., and Polepeddi, R. (2000). "Bridge rating with consideration for fatigue damage from overloads." *J. Bridge Eng.*, 10.1061/(ASCE)1084-0702(2000)5:3(259), 259–265.

Mohammadi, J., and Shah, N. (1992). "Statistical evaluation of truck overloads." *J. Transp. Eng.*, 10.1061/(ASCE)0733-947X(1992)118:5(651), 651–665.

Polepeddi, R. (1997). "The effect of fatigue damage in rating bridges under overload conditions." Ph.D. thesis, Illinois Institute of Technology, Chicago.

Raju, S., Moses, F., and Schilling, C. (1990). "Reliability calibration of fatigue evaluation and design procedures." *J. Struct. Eng.*, 10.1061/(ASCE)0733-9445(1990)116:5(1356), 1356–1369.

Schilling, C. (1984). "Stress cycles for fatigue design of steel bridges." *J. Struct. Eng.*, 10.1061/(ASCE)0733-9445(1984)110:6(1222), 1222–1234.

Schilling, C. G., and Klippstein, K. H. (1977). "Fatigue of steel beams by simulated bridge traffic." *J. Struct. Div.*, 105(1), 260–261.

Schilling, C. G., and Klippstein, K. H. (1978). "New method for fatigue design of bridges." *J. Struct. Div.*, 104(3), 425–438.

Schilling, C. G., Klippstein, K. H., Barsom, J. M., and Blake, G. T. (1978). "Fatigue of welded steel bridge members under variable-amplitude loadings." *National Cooperative Highway Research Program Rep. 188*, Transportation Research Board, Washington, DC.

Shi, X. M., Cai, C. S., and Chen, S. R. (2008). "Vehicle induced dynamic behavior of short-span slab bridges considering effect of approach slab condition." *J. Bridge Eng.*, 10.1061/(ASCE)1084-0702(2008)13:1(83), 83–92.

Snyder, R. E., Likins, G. E., and Moses, F. (1985). "Loading spectrum experienced by bridge structures in the United States." *Report No. FHWA/RD-85/012*, BridgeWeighing Systems Inc., Warrensville, OH.

Wang, T.-L., and Huang, D. (1993). "Computer modeling analysis in bridge evaluation-phase III." *Final Rep., Project No. FL/DOT/RMC/0542(3)-7851*, Florida Dept. of Transportation, Tallahassee, FL.

Wang, T.-L., and Liu, C. (2000). "Influence of heavy trucks on highway bridges." *Rep. No. FL/DOT/RMC/6672-379*, Florida Dept. of Transportation, Tallahassee, FL.

Wang, T., Liu, C., Huang, D., and Shahawy, M. (2005). "Truck loading and fatigue damage analysis for girder bridges based on weigh-in-motion data." *J. Bridge Eng.*, 10.1061/(ASCE)1084-0702(2005)10:1(12), 12–20.

Yang, Y.-B., Liao, S.-S., and Lin, B.-H. (1995). "Impact formulas for vehicles moving over simple and continuous beams." *J. Struct. Eng.*, 10.1061/(ASCE)0733-9445(1995)121:11(1644), 1644–1650.

Zhang, W., and Cai, C. (2012). "Fatigue reliability assessment for existing bridges considering vehicle speed and road surface conditions." *J. Bridge Eng.*, 10.1061/(ASCE)BE.1943-5592.0000272, 443–453.

Zhang, W., and Cai, C. (2013). "Reliability-based dynamic amplification factor on stress ranges for fatigue design of existing bridges." *J. Bridge Eng.*, 10.1061/(ASCE)BE.1943-5592.0000387, 538–552.

Zhao, J., and Tabatabai, H. (2012). "Evaluation of a permit vehicle model using weigh-in-motion truck records." *J. Bridge Eng.*, 10.1061/(ASCE)BE.1943-5592.0000250, 389–392.

Downloaded from ascelibrary.org by HUNAN UNIVERSITY on 11/07/16. Copyright ASCE. For personal use only; all rights reserved.